Journal of Inorganic Biochemistry 119 (2013) 75–84

Contents lists available at SciVerse ScienceDirect

Journal of Inorganic Biochemistry

journal homepage: www.elsevier.com/locate/jinorgbio

The key role of water in the dioxygenase function of *Escherichia coli* flavohemoglobin

Dardo N. Ferreiro [a,b], Leonardo Boechi [a], Darío A. Estrin [a,*], Marcelo A. Martí [a,b,**]

[a] Departamento de Química Inorgánica, Analítica y Química Física/INQUIMAE-CONICET, Facultad de Ciencias Exactas y Naturales, Universidad de Buenos Aires, Ciudad Universitaria, Pabellón 2, piso 1, C1428EHA, Buenos Aires, Argentina
[b] Departamento de Química Biológica, Facultad de Ciencias Exactas y Naturales, Universidad de Buenos Aires, Ciudad Universitaria, Pabellón 2, piso 4, C1428EHA, Buenos Aires, Argentina

ARTICLE INFO

Article history:
Received 1 June 2012
Received in revised form 31 October 2012
Accepted 31 October 2012
Available online 13 November 2012

Keywords:
Flavohemoglobin
Molecular dynamics
Protein electron transfer
Oxygen stabilization

ABSTRACT

Flavohemoglobins (FHbs) are members of the globin superfamily, widely distributed among prokaryotes and eukaryotes that have been shown to carry out nitric oxide dioxygenase (NOD) activity. In prokaryotes, such as *Escherichia coli*, NOD activity is a defence mechanism against the NO release by the macrophages of the hosts' immune system during infection. Because of that, FHbs have been studied thoroughly and several drugs have been developed in an effort to fight infectious processes. Nevertheless, the protein's structural determinants involved in the NOD activity are still poorly understood. In this context, the aim of the present work is to unravel the molecular basis of FHbs structural dynamics-to-function relationship using *state of the art* computer simulation tools. In an effort to fulfill this goal, we studied three key processes that determine NOD activity, namely i) ligand migration into the active site ii) stabilization of the coordinated oxygen and iii) intra-protein electron transfer (ET). Our results allowed us to determine key factors related to all three processes like the presence of a long hydrophobic tunnel for ligand migration, the presence of a water mediated hydrogen bond to stabilize the coordinated oxygen and therefore achieve a high affinity, and the best possible ET paths between the FAD and the heme, where water molecules play an important role. Taken together the presented results close an important gap in our understanding of the wide and diverse globin structural-functional relationships.

1. Introduction

Flavohemoglobins (FHbs) are members of the ubiquitous heme containing globin super family of proteins, which also includes the single domain globins and the truncated hemoglobins. Their characteristic fold combines an N-terminal globin domain (GD, residues 1 to ≈140), a FAD-binding domain (FBD, residues ≈140 to ≈250) and a NAD-binding domain (NBD, residues ≈250 to ≈400). These domains are organized in a "heart-shaped" structure, presenting a cleft in between the GD and the NBD (Fig. 1) [1,2]. Over the years, the discovery of novel globin genes among different types of organisms such as bacteria, algae, protozoa and fungi suggests that these proteins were not originally designed for oxygen transport and storage as the well known mammalian hemoglobin(Hb) and myoglobin(Mb) [3,4]. Instead, it has been proposed that they may perform a wide variety of tasks such as relief of nitro and oxidative stress; CO, NO or O_2 sensing; or even be involved in reductive and/or oxidative catalytic processes [3–5].

Particularly, FHbs have been suggested to play an important role in nitrosative stress resistance, due to their nitric oxide dioxygenase activity (NOD) [1,6]. This activity is also shared with other globins, such as some of the members of the truncated hemoglobins (also known as bacterial globins), like the *Mycobacterium tuberculosis* truncated hemoglobin N (MtTrHbN) [7–10]. Such function can make the difference between bacterial survival or death under stress conditions, as the attack of the hosts' immune system. Therefore, elucidating how FHbs carry out NOD activity is crucial for understanding bacterial resistance mechanisms. In this context, FHbs have been proposed as molecular targets for several antibacterial and antimycotic imidazole derived compounds, including the FDA approved azoles [11,12].

The NOD activity carried out by heme proteins consists in the conversion of nitric oxide (NO), which is toxic for the bacteria, into innocuous nitrate according to the NO detoxification reaction cycle, shown in Scheme 1 [9,13–16].

In order to perform NOD activity (see Scheme 1) the protein must be able to internalize O_2 into the GD and stabilize the iron bound oxygen, a process characterized by oxygen association and dissociation rate constants (k_{on} and k_{off}). Afterwards, the NO molecule must also migrate into the globin domain and react with the oxy-heme ($Fe^{II}O_2$) to form ferric heme (Fe^{III}) and a nitrate ion (NO_3^-) [9,14], which is then released to the solvent [17]. The NO reaction with oxy heme is usually characterized by the rate constant k_{ox}NO which is extremely fast. Finally, the protein needs to reduce the heme back

* Corresponding author.
** Correspondence to: M.A. Martí, Departamento de Química Inorgánica, Analítica y Química Física/INQUIMAE-CONICET, Facultad de Ciencias Exactas y Naturales, Universidad de Buenos Aires, Ciudad Universitaria, Pabellón 2, piso 1, C1428EHA, Buenos Aires, Argentina.
E-mail addresses: dario@qi.fcen.uba.ar (D.A. Estrin), marcelo@qi.fcen.uba.ar (M.A. Martí).

0162-0134/$ – see front matter © 2012 Elsevier Inc. All rights reserved.
http://dx.doi.org/10.1016/j.jinorgbio.2012.10.015

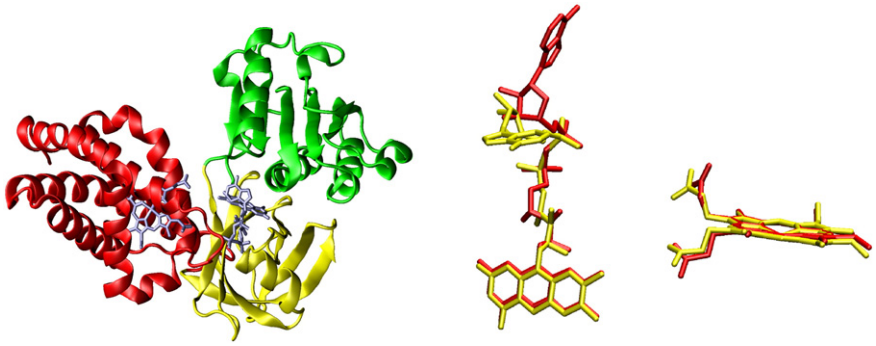

Fig. 1. Left panel: structure of *E. coli* flavohemoglobin. Red: globin domain. Yellow: FAD-binding domain. Green: NAD-binding domain. Right panel: FAD and heme crystal conformation. Red: A. eutrophus. Yellow: *E. coli*.

to the ferrous (Fe^{II}) state, usually through inter or intraprotein electron transfer (ET) from a suitable electron donor (***e***D) that is oxidized in one electron along the process, in order to start over the cycle [1].

Although possibly all globins may carry out NOD activity in-vitro under optimal conditions [16], not all of them are equally efficient. The most studied and well understood efficient NODs are the FHbs from *Escherichia coli, Alcaligenes eutrophus* and *S. cerevisae* [1,18,19], and the truncated hemoglobin MtTrHbN [7–10,17]. The structural elements that determine an efficient NOD activity have been related to fast ligand migration into the active site (O_2 into the deoxygenated protein and NO into the oxygenated protein) [8], strong stabilization of the oxygen coordinated to the heme [9], and fast electron transfer to recover the ferrous state [16].

To ensure fast NO incorporation into the oxygenated protein, and also for oxygen entry to the free protein, MtTrHbN relies on the presence of a tunnel cavity system which is allosterically modulated by the presence of the oxygen ligand [8,20]. All globins structurally studied so far reveal the presence of internal cavities and tunnels [21,22] which have been related to both ligand migration [23] and multi-ligand chemistry processes [24]. Interestingly, while in the truncated hemoglobins the tunnel/cavity system connects the heme active site with the solvent [22,8,20,25,26] in other globins the cavities do not connect the heme with the solvent, which is accessible through the so called HisE7 gate [23,24], but allow the ligand to go deeper inside the protein core [27]. So far, the way in which the ligand enters and exits the GD and how the tunnel/cavities for ligand migration are related to the global protein structure is unknown for FHbs.

In MtTrHbN, as in many globins, strong oxygen stabilization is ensured due to the presence of distal tyrosine at position B10 (TyrB10) which forms a tight hydrogen bond (HB) with the bound oxygen ligand [7,9]. Strikingly, although in FHbs position B10 is indeed occupied by a tyrosine, in the crystal structures (*E. coli* pdbid 1GVH [28], and *A. eutrophus* pdbid 1CQX [29]) TyrB10 is too far from the iron to establish an HB with the bound ligand. Moreover, in *A. eutrophus* FHb the crystal structure displays a phospholipid molecule with the lipid side chain inside the distal pocket, on top of the iron [29].

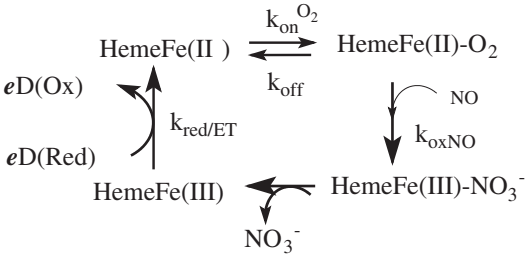

Scheme 1. Complete nitric oxide dioxygenase reaction cycle performed by heme proteins.

Given that no other HB donor residues are present in the distal pocket of FHb, the mechanism by which high oxygen affinity is achieved is still unclear. To complicate the picture even further, resonant Raman studies of CO bound *E. coli* FHb suggested the presence of two different conformations, which have been assigned to open and closed conformations of the distal pocket [30]. The closed conformation presents similar Fe–C and C–O vibrational frequency values as those reported for MtTrHbN where a tight HB is established with the CO ligand by TyrB10 [31], while the open conformation has vibrational frequencies which are similar to the H64V/V68T Myoglobin mutant [32] or the *T. tencogensis* HNOX domain [33] displaying an oxygen lone pair pointing towards the bound CO ligand [34]. Both conformations are supposed to be in dynamic equilibrium and increasing the environment pH increases the relative population of the open state [30].

Finally, what makes FHbs special over other globins, is the presence of the FBD and NBD, which ensures a fast and efficient heme reduction during catalytic turnover [1,2]. Heme reduction has been suggested to occur by shooting electrons from the co-substrate NAD to the FAD and, from there, to the heme; although direct NAD to heme electron transfer cannot be discarded. It is important to note, that since NAD is a two electron donor, while for each NOD cycle the globin domain requires only one electron, the Flavin not only acts an electron bridge, but allows the storing of one electron, after one re-reduction cycle. In other words, if the protein is completely oxidized and without NAD, once the NAD enters the protein it will first perform a two electron reduction of the FAD. Then one electron from the reduced Flavin will reduce the heme, while remaining in the semi reduced radical state, until the heme is oxidized after an NOD cycle. FHbs are thus unique globins, since reduction involves an intra-protein ET between domains, and not inter-protein ET, as is the case for Mb and Hb reduction by Cytochrome-b5 [35–37]. Although understanding how structure, dynamics and domain–domain interactions in FHbs modulate ET could give insights into general reduction mechanisms of globins, the molecular details of the ET process in FHbs are still unknown. The crystal structures of the *E. coli* flavohemoglobin (HMP) and the *Alcaligenes eutrophus* flavohemoglobin (FHP) lack the NAD co-substrate, but interestingly, in both of them, the FAD molecule adopts significantly different conformations, (Fig. 1) suggesting a high mobility of the adenine moiety [1,2].

The aim of the present work is to unravel the molecular basis of FHb structural dynamics-to-function relationship using *state of the art* computer simulation tools. To achieve this goal, we studied the three key processes that determine NOD activity, namely i) ligand migration and ii) oxygen binding and iii) intra-protein electron transfer. Our results allowed us to determine key factors related to all three processes like the presence of a long tunnel for ligand migration, the presence of a water mediated hydrogen bond to achieve a string stabilization for the ligand and therefore a high oxygen affinity, and the best possible ET paths between the FAD and the heme.

2. Computational methods

2.1. Set up of the system and equilibration

Protein coordinates were retrieved from the Protein Data Bank. The corresponding pdb code for *E. coli* flavohemoglobin is 1GVH (at 2.2 Å resolution), whose heme structure corresponds to Ferric pentacoordinated heme, which unexpectedly shows the distal site partially occupied by the isopropyl side chain Leu-E11, the Fe-LeuCG distance is 3.6 Å [28]. Starting from these structures, three systems were built, namely Deoxy_HMP, Oxy_HMP which is the same structure with oxygen added *in-silico* in the distal site, and CO_HMP which has a CO bound instead of an O_2. Both the ligand bound structures were first carefully optimized, allowing the Leu-E11 side chain to slightly move in order to accommodate the sixth ligand. Once the initial structures were constructed, the following thermalization and equilibration protocol was performed in explicit solvent for all the systems: hydrogens were added with the tleap module of the AMBER 9 program [38]. Standard protonation states were assigned to titratable residues (D and E are negatively charged, K and R positively charged). Histidine protonation was assigned favoring hydrogen bond formation whenever possible, while solvent exposed histidines where protonated in the epsilon position, since it corresponds to the most abundant tautomer in solution. The proximal Histidine F8 was protonated in the delta position, since the epsilon nitrogen is bound to the heme iron. The Flavin was simulated in the reduced state. Each protein was immersed in a truncated octahedral box of TIP3P water. After solvation, the systems consist of 396 aminoacids, a FAD molecule, a heme group, over 10,000 water molecules, and an oxygen molecule bound to the heme Fe for Oxy_HMP. Each system was optimized using a conjugate gradient algorithm for 2000 steps. This optimization was followed by 100 ps long constant volume MD thermalization in which the temperature of the system was slowly raised to 300 K. The heating was followed by a 100 ps long constant temperature and constant pressure MD simulation to equilibrate the system's density. During these processes the protein C_{alpha} atoms were restrained by a 10 kcal/mol harmonic potential for the thermalization and a 1 kcal/mol harmonic potential for the density equilibration.

2.2. MD simulations

80 ns and 40 ns long MD simulations, with no restraint for the C_{alpha} atoms, were performed for the oxygenated and deoxygenated protein (Oxy_HMP and Deoxy_HMP respectively). All MD simulations were performed using the PMEMD module of AMBER9 with the amber99SB force field parameters [39] for all residues except for the heme group. Heme parameters, for the three coordinated states (ferrous free, ferrous oxy and ferrous CO bond) were developed and thoroughly validated by our group in previous works, showing that they are able to accurately reproduce the structural and dynamical pattern of the distal site, particularly the protein ligand interactions [40–42]. Pressure and temperature were kept constant at 1 atm and 300 K with the Berendsen barostat and thermostat using standard protocols as implemented in AMBER [38]. All simulations were performed with periodic boundary conditions.

2.3. MD simulations with NAD co-substrate.

A 15 ns long additional simulation was performed, taking as a starting point a modified Deoxy_HMP snapshot. The above mentioned modification regards the inclusion of a NAD molecule into the NBD of *E. coli* FHb. Such inclusion was performed by aligning de Deoxy_HMP structure with cytochrome B5 reductase structure from *Rattus norvegicus* (pdb id: 1IB0) [43].

2.4. Determination and analysis of HMP tunnel cavity system for ligand migration

The Implicit Ligand Sampling [44] (ILS) approach is based in the calculation of the potential of mean force (PMF) corresponding to the placement of a small ligand inside each region of the whole protein matrix, in our case defined by a grid containing the globin domain. The corresponding PMF is associated to the free energy cost of incorporating the ligand at every point of the grid and therefore describes which regions of the protein are accessible to the ligand and the energy associated. The methodology relies on the fact that small ligands interact weakly with the protein matrix and therefore the interaction can be computed for protein structures that were obtained without the presence of the ligand in previous MD simulations. By performing the MD simulation of the protein without the ligand and treating its presence as a weak perturbation added afterwards, sampling of the ligand can be performed on the whole protein matrix simultaneously, from just one sufficiently long plain MD simulation [45]. In the present work ILS free energy profile is computed for the Oxy_HMP and Deoxy_HMP MD simulations, using 5000 snapshots and grid spacing of 0.5 Å.

2.5. Hybrid quantum/molecular mechanics calculations (QM/MM) simulations

Hybrid QM/MM simulations were performed using the HYBRID program developed in our group which combines a Density Functional Theory (DFT) based electronic structure method, with the Amber force field [46]. In this scheme, the quantum (QM) and the molecular mechanics (MM) subsystem are combined through a hybrid Hamiltonian. The protein (or classical) environment affects the electronic density in a self-consistent fashion due to the addition of the classical-point charge potential to the potential. The coupling term has two main contributions representing the electrostatic interaction between the electrons and nuclei, defining the QM charge density with the classical point charge and an additional term corresponding to the van der Waals and short range interactions between the atoms in the quantum and classical regions through a 6–12 Lennard–Jones potential. For all atoms, basis sets of double plus zeta polarization quality were employed with cut-off and energy shift values of 150 Ry and 25 meV. All calculations were performed using the generalized gradient approximation functional proposed by Perdew, Burke, and Ernzerhof [47] (PBE). For all systems the spin-unrestricted approximation was used. Only residues located within 10 Å from the heme reactive center were allowed to move freely in the QM/MM runs. The interface between the QM and MM portions of the system was treated with the scaled position link atom method. The hybrid program showed excellent performance for medium and large systems, and was proven to be appropriate for biomolecules, and particularly heme proteins as shown by several works from our group [40,42,48–52]. In the present case, the iron porphyrinate without the side chains, but with the relevant ligands, i.e. the proximal histidine and the oxygen molecule, were selected as the quantum subsystem. Heme spin states used for the calculations were: singlet for the hexacoordinated O_2 bound and CO bound hemes, quintuplet for the pentacoordinated heme, which are the experimentally known ground states for each system. All calculations, including those for the singlet states, were performed using the unrestricted spin approximation. The rest of the protein unit, together with water molecules, was treated classically, using the Amber99 force field parameterization.

Finally, we have performed QM/MM calculations of the O_2 binding energy, which is defined as:

$$\Delta E = E_{Heme-O2} - (E_{O2} + E_{Heme}) \quad (1)$$

where $E_{Heme\text{-}O2}$ is the energy of the oxy-form of the protein, E_{Heme} is the energy of the deoxy-form, and E_{O2} is the energy of the isolated

oxygen molecule. The initial structures for the QM/MM calculations were obtained from the MD simulations by cooling selected random snapshots to 0 K with a simulated annealing protocol. This scheme has been widely used by our group to compute the oxygen binding in several heme proteins, by showing that the computed oxygen binding energy (ΔE) exhibits a good correlation with the experimentally measured oxygen dissociation rate (k_{off}) [40,53–56].

2.6. Electron transfer pathway calculations

The pathway method provides an estimation of the ET rate, as characterized by the corresponding rate constant (k_{et}), which according to Marcus theory [57] for ET, is determined in the semi-classical regime by Eq. (2) shown below:

$$k_{et} = \frac{2\pi}{\hbar}|H_{AB}|^2 \frac{1}{\sqrt{4\pi\lambda k_b T}} \exp\left(-\frac{(\lambda + \Delta G^{\circ})^2}{4\lambda k_b T}\right) \quad (2)$$

As shown in the equation, the ET rate constant depends on three system dependent parameters, namely: the reaction standard free energy (ΔG^0), which is directly related to the difference in the donor acceptor redox potentials, the reorganization energy (λ), and the electronic coupling matrix element (H_{AB}). The other parameters being the Boltzmann constant (k_b), the Planck constant ($\hbar$) and the system temperature (T). The reorganization energy can be described as the energy required to shift (or convert) the system atomic coordinates from those corresponding to the minimum energy point for the reactants (i.e. when the electron is in the donor molecule) to those corresponding to the minimum energy point for the products (i.e. when the electron is located in the acceptor), but along the reactants energy surface (i.e. without the occurrence of the ET). The electronic coupling matrix element has no classical analogy but is directly related to the probability of occurrence of the ET step itself, in a given structure. For many cases of long range ET in proteins, H_{AB} is usually small and very important in the determination of the ET rate. Moreover, since in the present case we are dealing with the same protein system (including donor and acceptor cofactors), the reorganization energy and ET reaction free energy are constants. Therefore, to analyze the comparatively the ET step, the possible electron transfer paths were characterized by computing H_{AB} between the heme group and the FAD isoalloxazine ring, as estimated using the pathways algorithm. This algorithm, developed by Beratan et al. [58,59], was successfully used by our group for the study of the role played by protein dynamics on ET rates [60,61]. Briefly, the method looks for the best possible path that, with the highest H_{AB}, connects donor and acceptor selected orbitals. Orbitals are defined as either located on covalent bonds, or in free electron pairs as in oxygen atoms. This results, for example, in a water molecule displaying four orbitals with tetrahedral geometry, two corresponding to the O–H bonds and two corresponding to the free electron pairs. H_{AB} for a given pathway is computed as the product of a number of steps, each with a given coupling value, that define the pathway. A step can either be through atom, when two orbitals share an atom, which are assumed to have a coupling value of 0.6, and through space steps (or jumps) connecting orbitals separated by empty space, for which the coupling is assumed to decay exponentially with the orbital to orbital distance with a decay factor ($\beta = -1.7$) [58,59]. The H_{AB} reported value (in eV), is finally obtained by multiplying the obtained decay factor for the best ET path by 1 eV, which is the default value in the algorithm. To obtain a proper description of the system, minor adjustments of the parameters of the pathways algorithm were required. First, all orbitals of the heme iron were considered to be equivalent. Second, couplings between all porphyrin, FAD and NAD adenine rings and FAD isoalloxazine ring located orbitals were set to one in order to reproduce their resonant character. This parameter adjustment has already been successfully used by our group to study ET in heme proteins [60,61]. With the obtained parameters the following ET path and H_{AB} calculations were performed for each snapshot along the corresponding simulation: in oxygenated and deoxygenated HMP coupling pathways were calculated between the FAD isoalloxazine(donor) and the heme Fe atom(acceptor). For the simulation which also included the NAD co-substrate, three different pathways were computed i) from FAD isoalloxazine to the heme Fe atom, ii) from the NAD adenine to the FAD isoalloxazine groups, and iii) from the NAD adenine to the heme Fe atom. For comparison purposes we also computed the H_{AB} values using the approximation of Moser and Dutton [66], where the value decays exponentially with the distance between the redox centers, using an homogeneous and average decay factor ($\beta = -1.7$), independently of the type of structure that separates them.

3. Results

3.1. Stability of the simulations

The stability of the simulations was determined by analyzing the RMSD vs time plots (Fig. S1) for each system. All plots present RMSD values lower than 2.5 Å, being the oxygenated HMP, the system with the highest values. RMSF vs residue plots (data not shown) show low mobility for all the systems except for a few residues which are exposed to solvent. In summary, all systems remain stable during the timescale of the simulation and no significant changes are observed between the different coordination states, or due to NAD binding.

3.2. The ligand migration paths in HMP

We now turn our attention to the ligand migration process in HMP. As already mentioned, small molecule ligands usually access the active site iron of heme proteins either trough hydrophobic tunnels that connect the iron with the solvent as in truncated hemoglobins, or though residue gates as in myoglobin like globins. We analyzed the tunnel cavity system of HMP using the ILS method as described in the computational methods section, both for the oxygenated and deoxygenated systems, which presented very similar results and therefore only the Oxy_HMP is discussed. The method allows the fast determination of the secondary small ligand docking sites in proteins in remarkably good agreement with more costly free energy based methods and experimental data as recently shown in our group [45]. As shown in Fig. 2, HMP displays a tunnel that connects the heme active site (i.e. the distal pocket, DP) with the solvent, passing through three secondary docking sites (S1, S2 and S3) and spanning a distance of ~20 Å. The highest barrier corresponds to the passage from S2 to S1 which is of ca. 6 kcal/mol. The tunnel is lined by residues Phe110, Leu17, Leu106, Leu24, Phe58, Leu102, Ile61, from the solvent into the DP respectively, which as expected are all hydrophobic and consistent with the fact that no water is seen along the tunnel during the simulation.

Topologically the tunnel is oriented along the GD domain larger axis, pointing away from the domain-domain interaction surface and parallel to B and G. helices. It is connected to the solvent passing between helices A, G and H. The tunnel is equivalent to the long tunnel of truncated hemoglobins from the N and O group [8,27,58,59], and strikingly similar to the long tunnel of MtTrHbN (see Fig. S9 for a topological comparison). The MtTRHbN long tunnel is also oriented parallel to the B and G helices and connected to the solvent passing between helices A, G and H. Moreover in MtTrHbN also three secondary docking sites (Xe1, Xe2 and Xe3 are found). Two of them are close to the distal pocket in the same position as S1 found in HMP. This two sites cannot be found at the same time since their presence is dependent on the open/close conformation of the PheE15 gate residue. In the closed state, PheE15 blocks the access to the heme and the resulting Xe2 site lies just before it. In the open state, PheE15 occupies this cavity and a new deeper Xe3 site closer to the heme can be found [8–10]. In FHbs a Phe58 is found at position E15 present in ca. 40% of the sequences, and being replaced by smaller

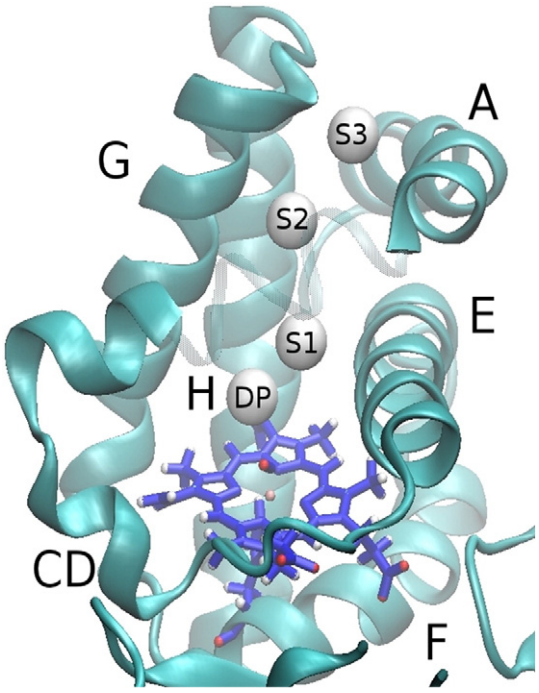

Fig. 2. Representation of the lowest free energy sites along the migration channel. Distal pocket, sites 1 through 3 is depicted, and globin domain helices labeled.

hydrophobic (mostly Ala) residues in the others. In our simulations Phe58 does however not act as a gate, but remains lining the S1 site. The other docking site found in MtTrHbN, Xe1, is equivalent to HMP S2 and finally the HMP S3 corresponds to the MtTrHb long tunnel entry, thus the tunnel is slightly shorter in the truncated (and smaller) globin.

An interesting feature of FHb is their ability to bind phospholipids, as clearly evidenced by the *A. eutrophus* crystal structure where a phospholipid molecule with the lipid side chain is found inside the distal pocket, on top of the iron [29]. Thus, in order to analyze the possible effect of lipid binding to the observed tunnel/cavity system we compared the FHb lipid bound structure to the HMP structure showing the secondary docking sites. As shown in Fig. S8, comparison of both structures, shows that the lipid side chain occupies a substantial portion of the DP and blocks the S1 docking site. This, fact could explain the lower k_{on} and k_{off} values determined for HMP in the presence of bacterial membrane lipid extracts [63].

3.3. Looking for the Structural determinants of HMP Oxygen Stabilization

As mentioned in the introduction, stability of iron coordinated oxygen is given mainly by distal site environment where usually key conserved residues such as HisE7, TrpG8 and TyrB10, act as hydrogen bond (HB) donors to the bound ligand [40,53] HMP contains a tyrosine in position B10 (TyrB10) and non HB forming residues in positions E7 (GlnE7) and G8 (ValG8). Strikingly, in *E. coli* crystal structure TyrB10 is too far from the Fe [28] (and in *A. eutrophus* it is even further) [29] to establish a HB with bound ligand, a fact that seemed inconsistent with both, the low observed k_{off} values, and the CO Resonance Raman frequency [18,30]. To understand the origin of oxygen stabilization in HMP we performed 80 ns of MD simulations of Oxy_HMP. During the initial phase of the simulation, which started with a dry distal pocked (DP), TyrB10 forms a HB with the ligand. However, after water molecules enter into the DP (about 15 ns into the simulation), one of the water molecules adopts a "bridge" conformation between TyrB10 and the oxygen ligand, establishing a tight "water mediated" HB which remains stable during the rest of the simulation time (Fig. 3). The entry of the water molecules in the active site is produced from the side of the heme propionates, which is closer to the bulk water. Thus water molecules enter from the opposite side of the hydrophobic tunnel. Once the waters are inside the DP, it never becomes dry again.

To characterize the structural and dynamical properties of the bridging water, we computed radial distribution probability functions ($g(r)$) for the water oxygen atom (O_w) using as the reference either the TyrB10 phenol oxygen atom (O_{OH}), or the distal oxygen atom (O_d) of the ligand (Fig. 2). Both plots show a sharp peak around 2.75 Å, which corresponds to the characteristic distance for a strong HB and shows that the water molecules have very small translational freedom, and therefore can be considered almost part of the structure. To analyze if the bridging water is able to rotate we computed the distance between Od and each of the water hydrogen atoms (H_{w1} and H_{w2}), the corresponding histogram probability distributions of the distance vs time plot (Fig. S2) clearly shows that each water hydrogen participates approximately 50% of the time in the HB, implying that water is free to rotate. Finally, we measured the time scale (i.e. the percentage of the simulated time) in which a tight hydrogen bond is established between the bridging water and the bound oxygen. Using a 3.5 Å distance cut-off for the oxygen atoms, and a O_d–H_w–O_w angle cut off of 150°, the HB is present 66% of the simulation time and has a maximum lifetime of 100 ps, values that drop to 12% and 40 ps for a 170° angle cut-off.

In summary, the bridging water is tightly bound inside the protein's active site, and therefore can be considered almost as a "structural water" and part of the protein, although it is exchanged with the bulk solvent and a tight HB with the bound oxygen is not present at all times. This can have, as will be shown below, deep implications for oxygen affinity. We also looked for the presence of water molecules in the ligand free protein. Visual inspection showed that in this case no tightly bound water is found in the active site and instead water molecules enter and escape the distal pocket (DP) easily. Leucine E11 has also significant mobility and occupies the DP on top of the heme during some segments of the simulation. TyrB10 also shows significant flexibility and alternates between two conformations interacting either with the backbone of the E helix or with the active site waters. Thus in the deoxygenated protein distal residues and water are highly mobile, thus not representing a significant hindrance to oxygen entry.

As explained above, TyrB10 is usually directly involved in HB with the bound ligand, as is the case for many globins [7,9,55,56]. Therefore, the fact that TyrB10 spontaneously forms a direct HB with the ligand within a few ns of simulation is very relevant. Nevertheless, as soon as water molecules penetrate into the DP, TyrB10 is displaced and stays in a "water-mediated" HB conformation for the rest of the simulation time. The latter fact implies that the direct HB of the former ns of the simulation might be an artifact due to the lack of water molecules inside the cavity. In summary, direct TyrB10 to oxygen HB is unlikely to be relevant since the water bridged conformation seems to be more stable.

Several other bacterial globins including Vitreoscilla hemoglobin [68] and the already mentioned MtTrHbN also show, as the presently studied HMP, a Gln in position E7, that could participate in hydrogen bonds to the bound ligands. In this context, our MD simulation results of the oxygenated protein show that in HMP GlnE7 adopts mostly an extended conformation, and is unable to establish hydrogen bond interactions with the bound ligand, thus preventing it from playing a pivotal role in oxygen stabilization. In this aspect HMP resembles Vitreoscilla hemoglobin, where kinetic studies on GlnE7 to Ala mutants showed little effect on the ligand binding properties [67,68].

To have a quantitative picture of the structural determinants for oxygen stabilization in FHbs, we performed QM/MM calculations of the oxygen binding energy (ΔE_{O2}) for three selected conformations of HMP taken from the above described MD simulations: a) TyrB10 HB to the bridging water molecule to the coordinated oxygen (Water HB)

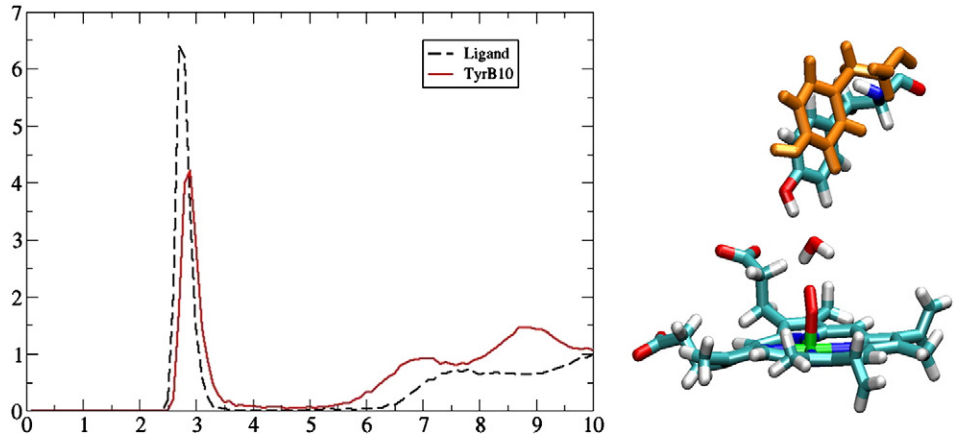

Fig. 3. Water mediated hydrogen bond. Left panel: translational radial distribution function g(r) plot for water molecules centered in: TyrB10 O_{OH} (red, solid line) and external coordinated O_2 (black, dashed line). Right panel: representative snapshot of water mediated hydrogen bond, where we superimpose TyrB10 after 20 ns of MD simulations (cyan, the back side upper middle structure) with TyrB10 before the simulation (orange, the front side upper middle structure).

b) TyrB10 direct HB to the coordinated O_2 (Direct HB) c) TyrB10 not interacting with the ligand (Not interacting). The average ± standard deviation ΔE_{O2} values, determined using three different starting snapshots derived from the oxyFHb MD simulation for each conformation, together with the previously obtained values for myoglobin and MtTrHbN, reported for comparative purposes, are shown in Table 1 (table with all obtained values is shown in SI).

Previous results from our group, have shown that QM/MM computed oxygen binding energy usually correlates with the oxygen dissociation rate (k_{off}) and therefore allows determining the structural reasons that control Fe – O_2 stabilization. Globins, with moderate dissociation rates (in the order of seconds) have show binding energies around 27–28 kcal/mol, like wt Mb, wt LegHemoglobin or TyrB10 to Ala mutant of MtTrHbN. Proteins, with higher dissociations rates, which almost do not bind oxygen have binding energies close or lower than 20 kcal/mol, like HE7G mutant Mb, or Cytochrome c'. Finally, heme proteins displaying low dissociation rates, i.e. below 1 s, have binding energies above 30 kcal/mol, like Ascaris hemoglobin, wt MtTrHbN or *Campilobacter Jejuni* Ctb [40,53–56]. The results from Table 1 show that only the water bridged (or direct HB) structure can explain the observed dissociation rate for HMP. When TyrB10 is far from the ligand (as in the crystal), the binding energy is too small, and even lower to that of Mb where the HisE7 is replaced by a non HB forming residue as Gly. Both the direct HB and water mediated HB show binding energies compatible with the low k_{off}, but given the instability of the direct HB conformation, the water bridged structure is more likely to represent the conformation in solution. In this context our results allow to solve the apparent contradiction between the crystallographic and kinetic studies. Moreover, the fact that two conformations (one with the bridging water and one without it) may be present on the protein, could explain the presence of two dissociation rates (i.e. biphasic kinetics) as observed by Bonamore et al. [1] Finally, the role played by the TyrB10 in holding the oxygen HB bound water in place, is also consistent with the experimental mutagenesis studies which show that mutation of TyrB10 to Phe increased the dissociation rate a hundred times [18].

To further corroborate the reliability of our results, we performed classical MD calculations with CO as the ligand. As mentioned in the introduction, CO bound resonant Raman measurements indicate the presence of a closed conformation with frequencies compatible with the presence of a tight HB to the ligand, and an open conformation where no strong HB is established. Moreover, increasing the pH results in an increase of the population of the open conformation [30]. Our MD simulations with bound CO show that, as for the oxygenated complex, a conformation with a bridging water HB to the bound CO is present during a significant portion of the simulation time (Fig. S5). However, and as expected due to its lower HB acceptor characteristics of the CO ligand as compared to O_2, the HB is also absent during a considerable amount of the simulation time. HB analysis for the CO bound protein showed that the HB is formed 20% of the simulation time and the maximum lifetime is 30 ps. These results strongly suggest assigning the closed conformation to that with the bridging water, while the open conformation would correspond to those where no water or no HB to the ligand is present. To further validate our assignation of the open and closed structures, we looked at the observed pH effect. The apparent transition pKa was determined to

Table 1
Binding energy values for O_2 as obtained from the QM/MM calculations.

Protein	HMP			Mb	MbHE7G	MtTrHbN
Conformation	Water HB	Direct HB	Not interacting			
ΔE_{O2}	−30.79 ± 2.79	−30.13 ± 0.73	−20.04 ± 2.11	−27.0	−22.7	−37.2
d(Fe-O)	1.77	1.79	1.77	1.84	1.76	1.84
$d(O_p\text{-}O_d)$	1.31	1.31	1.29	1.30	1.28	1.31
qO_2	−0.34	−0.42	−0.25	−0.22	−0.22	−0.36
$d(Fe\text{-}N_{His})$	2.18	2.10	2.13	2.18	2.18	2.06
dHB	2.72	2.73	5.56	2.99	–	2.75
k_{off} (s^{-1})	0.44[a], 0.11(56%), 2.2(44%)[b]			12	1600	0.2
Refs	(a) [18,19]; (b) [1]			[23,40,53]	[23,40,53]	[9,40]

ΔE_{O2} is the oxygen binding energy (in kcal/mol). For HMP average ± standard deviation values determined for calculation of three independent optimized structures derived from initial random selected snapshots taken from the MD simulation are presented. d(Fe – O), d(Op – Od), $d(Fe - N_{His})$ and dHB are the iron-oxygen, $O_{proximal} - O_{distal}$, Iron–proximal histidine and distal hydrogen bond distances in Angstroms. qO_2 is the O_2 Mulliken charge in units of electron, k_{off} is the experimentally determined oxygen dissociation rate constant. a,b Correspond to two different experimental determinations of k_{off} performed by different groups, as described in references [18,19,1] respectively.

be 8.3 [30], a value which is not too far form the Tyrosine pKa in solution (ca. 10). Based on this data and the fact that TyrB10 is responsible for holding the bridging water and the only titrable residue close to the active site, we performed MD simulations of the oxy and CO complex with a charged TyrB10. Interestingly, and consistent with our hypothesis, once TyrB10 is deprotonated it swings out from the active site (See Fig. S6) and therefore water can no longer be tightly hydrogen bonded to the bound ligand. The deprotonated TyrB10 is mainly interacting with solvent and with Arg48 of the CD loop, an interaction that could lower the apparent pKa to the observed values. Finally, it should be noted that the presence of an open and closed conformations is also consistent with the biphasic behavior of k_{off} described in Table 1.

In summary, results for the CO bound protein, corroborate the reliability of our simulations and allow assignment of the bridging water to ligand HB conformation to the closed conformation, while the dry or non HB conformation will correspond to the so-called open conformation.

Finally, we decided to look at the conservation of the analyzed residues in several sequences of FHb. Analysis of the multiple alignment of all sequences displaying a GB–FBD–NBD domain structure (not shown), shows that key TyrB10 is present in 96% of the sequences. Interestingly, GlnE7 is also highly conserved 95%, while the Val at position G8 is not, and in other FHbs a Trp is found.

3.4. Electron transfer pathways

Finally, we turn our attention to the reduction step, which relies on the calculations of possible ET paths and electronic coupling (H_{AB}) values as computed with the pathways algorithm, which is described in the computational methods section. The method looks for the best possible structural path that, with the highest H_{AB}, connects donor and acceptor. Thus the method allows to compare which structural elements (and their behavior along the dynamics) are critical for ET. The computed H_{AB} values should be considered only as an estimation of the real coupling values, but, as shown in previous works from our group [60,61] and others [58,59,62,69–73], are accurate enough to distinguish and characterize different possible ET paths in the same protein, and/or preferred ET conformations, in remarkable consistency with experimental measurements of the ET rates [58,59,62,69–73]. Moreover, since in the present case donor and acceptor states are the same for all studied cases, since we are dealing with the same protein, the other factors governing ET, like the reorganization energy, and ET reaction free energy, remain constant.

We begin our analysis by computing the electron transfer coupling from the FAD molecule (isoalloxazine ring) to the heme group (Fe atom) for each snapshot along the whole simulations. The results for the average, maximum and standard deviation of the corresponding values are presented in Table 2. The data show that protein explicit solvation and dynamics significantly affect ET path and coupling, and allow the protein to sample conformations with significant higher coupling values as compared to those that can be obtained from the crystal structures. Values along the dynamics are more than 10 times higher than those found in the *E. coli* X-ray structure, (which are already higher than those for *A. eutrophus*) which would result in 100 times faster ET rate, according to the Marcus theory. This result is from the general viewpoint of the dynamic and solvent role in ET process in proteins, in good agreement with previous observations from our group in other systems [61].

The origin of this difference is, as will be described below, due to dynamical and solvation related aspects. In *E. coli* X-ray structure the best ET path goes from the isoalloxazine ring to Gln205 of the FBD and jumps to Lys84 located in the HD F-helix and from there to the heme (data not shown). On the other hand, during the simulation, the high mobility of the FAD adenine moiety allows it to come closer to both the isoalloxazine ring and the heme group, which results in the formation of a transient conformation where the FAD-adenine-NH_2 group interacts with the heme-propionate through water bridged hydrogen bonds. This conformation allows for a high coupling path to be established which connects FAD isoalloxazine directly to the FAD adenine and from there to heme through the bridging waters (Fig. 4). The water molecules involved in bridging the adenine with the heme group are not fixed in that position, on the contrary, that space is accessible to bulk water and therefore the water exchange is frequent.

Table 2
Electron transfer coupling values and statistics.

Structure/Conformation	$< H_{AB} >$	Max H_{AB}	H_{AB} SD	Dutton H_{AB}
FAD=>HEM				
HMP X-ray	7.1×10^{-5}			1.9×10^{-8}
FHP X-ray	6.1×10^{-6}			1.2×10^{-9}
Oxy_HMP whole MD (80 ns)	8.0×10^{-4}	1.7×10^{-2}	7.4×10^{-4}	1.9×10^{-8}
Oxy_HMP HC segment (10 ns)	1.5×10^{-3}	1.7×10^{-2}	1.6×10^{-3}	3.4×10^{-8}
Oxy_HMP LC segment (70 ns)	7.0×10^{-4}	3.8×10^{-3}	4.3×10^{-4}	1.6×10^{-8}
Whole MD with NAD(15 ns)	1.0×10^{-3}	8.9×10^{-3}	9.5×10^{-4}	4.2×10^{-8}
NAD=>FAD				
Whole MD with NAD(15 ns)	5.0×10^{-3}	4.9×10^{-2}	5.1×10^{-3}	1.0×10^{-5}
NAD=>HEM				
Whole MD with NAD(15 ns)	9.3×10^{-4}	7.3×10^{-3}	8.8×10^{-4}	1.9×10^{-10}

$<H_{AB}>$, Max H_{AB} and H_{AB} SD are the mean, maximum and standard deviation values, in units of eV. HC and LC stand for High Coupling and Low Coupling respectively. FAD-HEM, NAD–FAD and NAD–HEM are the calculations performed, i.e. FAD–HEM signifies that the electron pathway was defined to start from FAD molecule and end in the heme group. Dutton H_{AB} corresponds to the computed H_{AB} using the approximation of Moser and Dutton[66] as described in methods.

Due to the above mentioned mobility of the FAD adenine moiety we looked closely for the relationship between FAD adenine conformation and the ET path and coupling values. Visual analysis of the simulation shows that FAD may adopt two significantly different conformations characterized by the distance between the isoalloxazine and adenine parts of the FAD molecule, and with different characteristic coupling values. As shown in Fig. 4, when both fragments of the FAD are further apart, ca. 6–9 Å the protein is in the low coupling (LC) regime, with average coupling values of 7.1×10^{-4} eV (still 10 times higher than the calculated coupling for the X-ray structure). When the adenine moiety comes closer to the isoalloxazine ring, to ≈4.5 Å, the protein temporarily enters the high coupling (HC) regime, where coupling values can be as high as 1.7×10^{-2}. Finally, in order to analyze the possible role of the protein structure and dynamics with FAD conformation, we analyzed the interactions between the adenine moiety in both conformations, and the protein matrix. Visual inspection of the dynamics show that in the LC regime the adenine moiety is mostly solvent exposed and that can be trapped in this conformation by strong hydrogen bond interaction with Glu223 of the FBD. In the HC conformation, the adenine comes closer to the heme propionates establishing the "electronic bridge" and partially interacting with Gln204 of the FBD.

To confirm the relationship between FAD conformation and high coupling, we also performed a constrained MD simulation in which the system was forced to remain in the HC conformation (two constraints were applied, namely: isoalloxazineC9-adenineC2A and adenineN6A-hemepropionateCGD atoms were held at a distance of 3.94 Å and 4.85 Å respectively for 10 ns and then released). The results, presented in Fig. S4, confirm the strong correlation between FAD conformation and coupling, since the values remain high when the FAD is forced to the HC conformation, and decay once it is released. Interestingly, the decay of the coupling values, once the constraint is released, is not to basal LC values. Nevertheless, the decay would be expected to enter the LC regime as the distance between the adenine and isoalloxazine moieties elongates. For comparison purposes we also computed the predicted coupling values using the Dutton approximation, that assumes that the value decays exponentially with the distance between the redox centers with an homogeneous and average decay factor. As expected, with this approximation, no difference is observed between

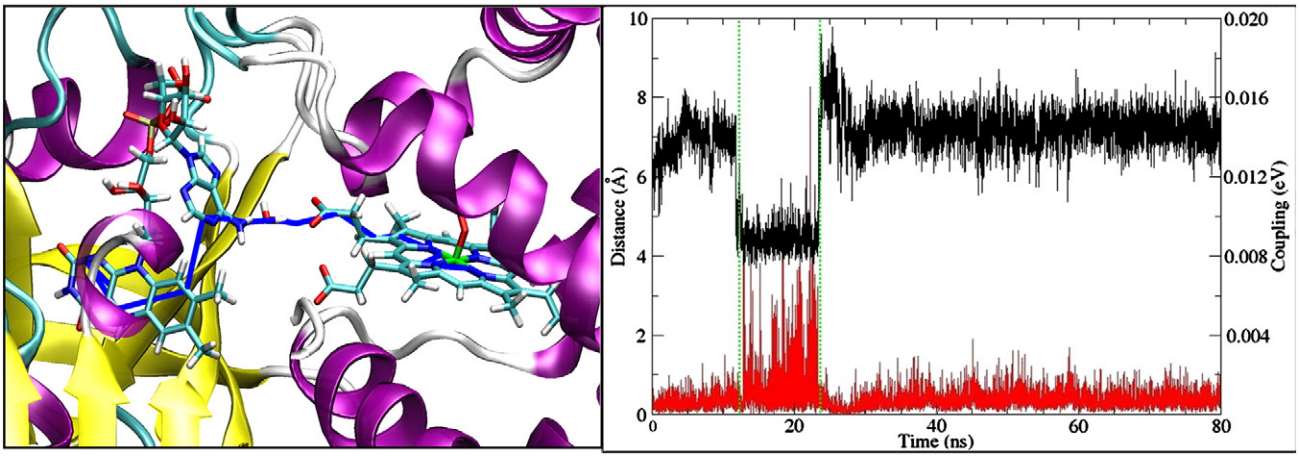

Fig. 4. Left panel: C(HC) microconformation in the protein context. Relevant water molecules are depicted. Blue line represents electron path. Right panel: electron transfer coupling in *E. coli* flavohemoglobin for oxygenated protein is shown in red, distance between adenine-C2A atom and isoalloxazine-C9 atom is shown in black. C(HC) microconformation corresponds to the portion comprised by the green dotted vertical lines.

the crystal structure and MD coupling values, since the FAD heme distance remains fairly constant along the simulation. Also, the differences between the LC and HC regimes are much smaller, for the maximum possible coupling values. Another observation comparing both the Beratan and Dutton models is that coupling values obtained with the pathway algorithm are significantly higher than those obtained with the Dutton model. Two reasons could account for the observed differences. First, as shown in Table 2, in the present case the largest differences between the methods are observed when the results are compared using the snapshots taken from the MD simulation, where a key water and the observed FAD small conformational changes results in a specific high coupling ET path, which are not considered in the simplified Dutton model. Another reason for the observed difference may lay in the fact that in the present case both the heme and FAD aromatic ring couplings in the pathway algorithm were set to 1, thus decreasing the number of steps needed to bridge the two redox centers. In any, case and despite the differences in the absolute computed H_{AB} values, these results highlight the relevance of particular microconformations for the ET process, as also shown by us in previous works for cytochrome-c [61].

To complete the ET picture in the reduction process, we also studied HMP containing a co-substrate NAD molecule. The corresponding structure was built, using cytochrome b5 reductase as the reference of a NAD bound domain, (as described in computational methods) and subject to 15 ns long MD simulations. The resulting analysis of the coupling calculations are also presented in Table 2. The results show that NAD and FAD molecule are coupled with very high values that ensure an efficient ET process between them. Visual inspection of the best ET path shows that the electron goes through mostly one (sometimes two) water molecules (Fig. 4), highlighting again the relevance of solvent structure for the ET process. Finally, we analyzed the coupling between NAD and heme cofactors. The results show that NAD to heme H_{AB} values are similar on average than those found for FAD to heme ET, although they are slightly lower than those found for the FAD to heme when the adenine remains in the HC conformation. These results suggest that direct NAD to heme ET could kinetically compete with FAD to heme ET. Overall, these results clearly show the relevance of protein dynamics (especially regarding the FAD molecule) and the presence of solvent molecules for the ET process.

4. Discussion

4.1. Ligand migration paths in HMP

Using the ILS method [44] we were able to find a tunnel that connects the HMP active site with the solvent which closely resembles the long tunnel found in group N and O TrHbs [8,20,22]. It is interesting to remark that globins of the 3-over-3 structural type, to which FHbs GD belongs, like Mb, neuroglobin, and cytoglobin, usually display an internal cavity system consisting of several (usually four) so called Xenon sites, that connect the heme distal proximal sites with no clear connection to the solvent, and which is significantly different topologically from the TrHbs long tunnel. In this context, the fact that FHb hosts a tunnel that is at odds with other structural similar globins, highlights the plasticity of the globin domain structure to adapt the internal cavity towards its need, and supports the notion that a direct tunnel connecting the solvent with the heme is important for NOD activity, as observed in MtTrHb [8].

4.2. Oxygen stabilization

Since the first kinetic characterization of HMP it was clear that this protein had very strong oxygen stabilization, compatible with the role as NOD and not as an oxygen carriage or storage protein, and with the conserved TyrB10 playing a predominant role, as observed for MtTrHbN [18]. Strikingly the crystal structures of HMP and FHP showed that TyrB10 was too far away from the iron to establish an HB bond and stabilize the bound ligand [28,29]. Our results for the oxygenated protein dynamics and oxygen binding energy reconcile this contradiction and show that TyrB10 is responsible for the low observed oxygen dissociation rates, by means of a water bridged HB interaction. The obtained values for the oxygen binding energies are consistent with past results in hemeproteins from our group [40,53–56] and help to understand in a quantitative manner the nature of oxygen binding in FHbs. It is important to point out that this is the first time that a water bridged hydrogen bond has been found and described in a globin (though it has been shown to be relevant in peroxidases [63]). So, the question arises, why is TyrB10 in FHbs crystals too far from the heme to interact directly with the ligand as observed in many other globins? We propose that the flexibility of the distal cavity size that is obtained with a water bridged HB to stabilize bound oxygen may allow FHbs to perform other functions that require a wider distal cavity space but nonetheless be able to coordinate oxygen tightly, through the water adaptor, to perform NOD activity. In particular FHbs have been shown to posses alkylhydroperoxide reductase activity [64], which taken together with the unique lipid-binding properties of HMP and the crystal structure of FHP which presents a phospholipid bound to the heme, would explain the need of these proteins for a wider distal pocket. In summary the flexibility of the distal cavity achieved through the water bridge could be related FHbs as being multifunctional enzymes.

4.3. Electron transfer pathways

Our analysis for the possible ET path show several interesting results. The first point concerns the active role played by FAD intrinsic dynamics which shows that high coupling structures are obtained due to FAD movement and presence of water molecules that bridge the ET path between both domains (FBD and GD). The key role of structural bridging waters for FHb ET paths is consistent with previous results reported by several groups who showed that water molecules are able to adapt protein contact surfaces of ET transfer complexes significantly enhancing the corresponding rate [62,69–73]. Other relevant point concerns the electron entry point on the GD. Most (if not all) members of the globin family must be reduced in order to accomplish their function. In most cases reduction is performed by another protein (the electron donor) that reduces the heme through interprotein ET. For the extensively studied mammalian Mb and Hb the reduction partner is Cytochrome-b5 (Cb5) another small heme protein [35–37,65]. An interesting question then arises as if the electron entry point to the globin domain is similar in interprotein (Mb/Cb5) and intraprotein (GD/FBD) ET. Our results show that in FHb the electron enters the GD through the heme propionates. Interestingly, the results for the Mb/Cb5 show that best ET paths are those were electrons enter directly to Mb though the heme exposed edge which includes the propionates [35–37,65]. Although so far only these two cases have been analyzed and there is a complete lack of knowledge of many globin (particularly bacterial globins) reduction partners, it is tempting to propose that redox partners should dock close to the heme exposed edges for efficient ET to occur. Regarding the electron entry point, we also looked for residue conservation in the GD/FBD interface in multiple alignments of Fhb proteins. The results show that both residues envolved in FAD conformation Gln205 and Glu224 are highly conserved, being present in ca 70% of the sequences, and being replaced mainly by Asparagine (or in some cases Histidine) and Aspartic acid (i.e. conservative mutantions) in most of the other cases. Thus the hydrophilic and negative charge properties of these residues are a conserved and possibly important feature of the FHb family.

5. Conclusions

Using computer simulation techniques we studied the molecular basis for *E. coli* FHb NOD activity. Our results showed that i) A hydrophobic tunnel topologically similar to that found in truncated hemoglobins N and O connects the heme active site with solvent, therefore promoting ligand migration ii) a strong oxygen stabilization is achieved due to a TyrB10 through water bridged hydrogen bond interaction. and iii) ET path depends strongly on the FAD conformation and the presence of bridging water molecules between the FBD and GD, while electrons enter the GD directly through the heme propionates as in Mb/Cytochrome-b5 ET transfer. Taken together the presented results close an important gap in our understanding of the wide and diverse globin structural-functional relationships.

Abbreviations

Mb	myoglobin
FHbs	Flavohemoglobins
NOD	nitric oxide dioxygenase
HMP	flavohemoglobin from *Escherichia coli*
FHP	flavohemoglobin from *Alcaligenes eutrophus*
ET	electron transfer
FDA	food and drug administration
QM–MM	quantum mechanics–molecular mechanics
MD	molecular dynamics
ILS	implicit ligand sampling
MSMD	multiple steering molecular dynamics
DFT	density functional theory

Acknowledgements

This work was supported by grants PICT-2010-0416, UBACyT 2010/2012, PIP 12-200801-01207 and Subsidio Bunge y Born para enfermedades infecciosas to MAM; DAE and MAM are members of CONICET.

Appendix A. Supplementary data

Supplementary data to this article can be found online at http://dx.doi.org/10.1016/j.jinorgbio.2012.10.015.

References

[1] A. Bonamore, A. Boffi, IUBMB Life 60 (2008) 19–28.
[2] A. Ilari, A. Boffi, Meth. Enzymol. 436 (2008) 187–202.
[3] S.N. Vinogradov, D. Hoogewijs, X. Bailly, R. Arredondo-Peter, J. Gough, S. Dewilde, L. Moens, J.R. Vanfleteren, BMC Evol. Biol. 6 (2006) 31.
[4] S.N. Vinogradov, D. Hoogewijs, X. Bailly, R. Arredondo-Peter, M. Guertin, J. Gough, S. Dewilde, L. Moens, J.R. Vanfleteren, Proc. Natl. Acad. Sci. U. S. A. 102 (2005) 11385–11389.
[5] R. Baron, J.A. McCammon, A. Mattevi, Curr. Opin. Struct. Biol. 19 (2009) 672–679.
[6] A.M. Gardner, P.R. Gardner, J. Biol. Chem. 277 (2002) 8166–8171.
[7] H. Ouellet, Y. Ouellet, C. Richard, M. Labarre, B. Wittenberg, J. Wittenberg, M. Guertin, Proc. Natl. Acad. Sci. U. S. A. 99 (2002) 5902–5907.
[8] A. Bidon-Chanal, M.A. Martí, A. Crespo, M. Milani, M. Orozco, M. Bolognesi, F.J. Luque, D.A. Estrin, Proteins 64 (2006) 457–464.
[9] A. Crespo, M.A. Martí, S.G. Kalko, A. Morreale, M. Orozco, J.L. Gelpi, F.J. Luque, D.A. Estrin, J. Am. Chem. Soc. 127 (2005) 4433–4444.
[10] A. Lama, S. Pawaria, A. Bidon-Chanal, A. Anand, J.L. Gelpí, S. Arya, M. Martí, D.A. Estrin, F.J. Luque, K.L. Dikshit, J. Biol. Chem. 284 (2009) 14457–14468.
[11] R.A. Helmick, A.E. Fletcher, A.M. Gardner, C.R. Gessner, A.N. Hvitved, M.C. Gustin, P.R. Gardner, Antimicrob. Agents Chemother. 49 (2005) 1837–1843.
[12] E. El Hammi, E. Warkentin, U. Demmer, F. Limam, N.M. Marzouki, U. Ermler, L. Baciou, Biochemistry 50 (2011) 1255–1264.
[13] E. De Marinis, L. Casella, C. Ciaccio, M. Coletta, P. Visca, P. Ascenzi, IUBMB Life 61 (2009) 62–73.
[14] E.T. Yukl, S. de Vries, P. Moënne-Loccoz, J. Am. Chem. Soc. 131 (2009) 7234–7235.
[15] P.R. Gardner, A.M. Gardner, W.T. Brashear, T. Suzuki, A.N. Hvitved, K.D.R. Setchell, J.S. Olson, J. Inorg. Biochem. 100 (2006) 542–550.
[16] B.J. Smagghe, J.T. Trent III, M.S. Hargrove, PLoS One 3 (2008) e2039.
[17] M.A. Martí, A. Bidon-Chanal, A. Crespo, S.-R. Yeh, V. Guallar, F.J. Luque, D.A. Estrin, J. Am. Chem. Soc. 130 (2008) 1688–1693.
[18] A.M. Gardner, L.A. Martin, P.R. Gardner, Y. Dou, J.S. Olson, J. Biol. Chem. 275 (2000) 12581–12589.
[19] P.R. Gardner, A.M. Gardner, L.A. Martin, Y. Dou, T. Li, J.S. Olson, H. Zhu, A.F. Riggs, J. Biol. Chem. 275 (2000) 31581–31587.
[20] M. Milani, A. Pesce, Y. Ouellet, P. Ascenzi, M. Guertin, M. Bolognesi, EMBO J. 20 (2001) 3902–3909.
[21] M. Brunori, Q.H. Gibson, EMBO Rep. 2 (2001) 674–679.
[22] M. Milani, A. Pesce, Y. Ouellet, S. Dewilde, J. Friedman, P. Ascenzi, M. Guertin, M. Bolognesi, J. Biol. Chem. 279 (2004) 21520–21525.
[23] E.E. Scott, Q.H. Gibson, J.S. Olson, J. Biol. Chem. 276 (2001) 5177–5188.
[24] R. Elber, Curr. Opin. Struct. Biol. 20 (2010) 162–167.
[25] L. Boechi, M.A. Martí, M. Milani, M. Bolognesi, F.J. Luque, D.A. Estrin, Proteins 73 (2008) 372–379.
[26] L. Boechi, P.A. Mañez, F.J. Luque, M.A. Marti, D.A. Estrin, Proteins 78 (2010) 962–970.
[27] B.P. Schoenborn, J. Mol. Biol. 45 (1969) 297–303.
[28] A. Ilari, A. Bonamore, A. Farina, K.A. Johnson, A. Boffi, J. Biol. Chem. 277 (2002) 23725–23732.
[29] U. Ermler, R.A. Siddiqui, R. Cramm, B. Friedrich, EMBO J. 14 (1995) 6067–6077.
[30] M. Mukai, C.E. Mills, R.K. Poole, S.R. Yeh, J. Biol. Chem. 276 (2001) 7272–7277.
[31] M. Couture, S.R. Yeh, B.A. Wittenberg, J.B. Wittenberg, Y. Ouellet, D.L. Rousseau, M. Guertin, Proc. Natl. Acad. Sci. U. S. A. 96 (1999) 11223–11228.
[32] G.N. Phillips, M.L. Teodoro, T. Li, B. Smith, J.S. Olson, J. Phys. Chem. B 103 (1999) 8817–8829.
[33] D.S. Karow, D. Pan, R. Tran, P. Pellicena, A. Presley, R.A. Mathies, M.A. Marletta, Biochemistry 43 (2004) 10203–10211.
[34] L. Capece, D.A. Estrin, M.A. Marti, Biochemistry 47 (2008) 9416–9427.
[35] P. Xiong, J.M. Nocek, J. Vura-Weis, J.V. Lockard, M.R. Wasielewski, B.M. Hoffman, Science 330 (2010) 1075–1078.
[36] J.M. Nocek, A.K. Knutson, P. Xiong, N.P. Co, B.M. Hoffman, J. Am. Chem. Soc. 132 (2010) 6165–6175.
[37] K.E. Wheeler, J.M. Nocek, D.A. Cull, L.A. Yatsunyk, A.C. Rosenzweig, B.M. Hoffman, J. Am. Chem. Soc. 129 (2007) 3906–3917.
[38] D.A. Case, *AMBER 11*, University of California, San Francisco, 2010.
[39] V. Hornak, R. Abel, A. Okur, B. Strockbine, A. Roitberg, C. Simmerling, Proteins 65 (2006) 712–725.
[40] M.A. Marti, A. Crespo, L. Capece, L. Boechi, D.E. Bikiel, D.A. Scherlis, D.A. Estrin, J. Inorg. Biochem. 100 (2006) 761–770.

[41] D.E. Bikiel, L. Boechi, L. Capece, A. Crespo, P.M. De Biase, S. Di Lella, M.C. González Lebrero, M.A. Martí, A.D. Nadra, L.L. Perissinotti, D.A. Scherlis, D.A. Estrin, Phys. Chem. Chem. Phys. 8 (2006) 5611–5628.
[42] M.A. Marti, L. Capece, A. Bidon-Chanal, A. Crespo, V. Guallar, F.J. Luque, D.A. Estrin, Meth. Enzymol. 437 (2008) 477–498.
[43] M.C. Bewley, C.C. Marohnic, M.J. Barber, Biochemistry 40 (2001) 13574–13582.
[44] J. Cohen, K.W. Olsen, K. Schulten, Meth. Enzymol. 437 (2008) 439–457.
[45] F. Forti, L. Boechi, D.A. Estrin, M.A. Marti, J. Comput. Chem. 32 (2011) 2219–2231.
[46] A. Crespo, D.A. Scherlis, M.A. Martí, P. Ordejón, A.E. Roitberg, D.A. Estrin, J. Phys. Chem. B 107 (2003) 13728–13736.
[47] J.P. Perdew, K. Burke, M. Ernzerhof, Phys. Rev. Lett. 77 (1996) 3865.
[48] A. Crespo, M.A. Martí, A.E. Roitberg, L.M. Amzel, D.A. Estrin, J. Am. Chem. Soc. 128 (2006) 12817–12828.
[49] M.A. Martí, L. Capece, A. Crespo, F. Doctorovich, D.A. Estrin, J. Am. Chem. Soc. 127 (2005) 7721–7728.
[50] M.A. Martí, A. Crespo, S.E. Bari, F.A. Doctorovich, D.A. Estrin, J. Phys. Chem. B 108 (2004) 18073–18080.
[51] L. Capece, A. Lewis-Ballester, D. Batabyal, N. Di Russo, S.-R. Yeh, D.A. Estrin, M.A. Marti, J. Biol. Inorg. Chem. 15 (2010) 811–823.
[52] A. Lewis-Ballester, D. Batabyal, T. Egawa, C. Lu, Y. Lin, M.A. Marti, L. Capece, D.A. Estrin, S.-R. Yeh, Proc. Natl. Acad. Sci. U. S. A. 106 (2009) 17371–17376.
[53] L. Capece, M.A. Marti, A. Crespo, F. Doctorovich, D.A. Estrin, J. Am. Chem. Soc. 128 (2006) 12455–12461.
[54] M.A. Martí, L. Capece, D.E. Bikiel, B. Falcone, D.A. Estrin, Proteins 68 (2007) 480–487.
[55] P. Arroyo Mañez, C. Lu, L. Boechi, M.A. Martí, M. Shepherd, J.L. Wilson, R.K. Poole, F.J. Luque, S.-R. Yeh, D.A. Estrin, Biochemistry 50 (2011) 3946–3956.
[56] M.A. Martí, D.E. Bikiel, A. Crespo, M. Nardini, M. Bolognesi, D.A. Estrin, Proteins 62 (2006) 641–648.
[57] R.A. Marcus, J. Chem. Phys. 24 (1956) 966–978.
[58] D.N. Beratan, J.N. Onuchic, J.R. Winkler, H.B. Gray, Science 258 (1992) 1740–1741.
[59] D.N. Beratan, J.N. Betts, J.N. Onuchic, Science 252 (1991) 1285–1288.
[60] H.K. Ly, M.A. Marti, D.F. Martin, D. Alvarez-Paggi, W. Meister, A. Kranich, I.M. Weidinger, P. Hildebrandt, D.H. Murgida, Chemphyschem 11 (2010) 1225–1235.
[61] D. Alvarez-Paggi, D.F. Martín, P.M. DeBiase, P. Hildebrandt, M.A. Martí, D.H. Murgida, J. Am. Chem. Soc. 132 (2010) 5769–5778.
[62] I.M.C. van Amsterdam, M. Ubbink, O. Einsle, A. Messerschmidt, A. Merli, D. Cavazzini, G.L. Rossi, G.W. Canters, Nat. Struct. Biol. 9 (2002) 48–52.
[63] G. Smulevich, A. Feis, B.D. Howes, Acc. Chem. Res. 38 (2005) 433–440.
[64] A. Bonamore, P. Gentili, A. Ilari, M.E. Schininà, A. Boffi, J. Biol. Chem. 278 (2003) 22272–22277.
[65] Z.-X. Liang, I.V. Kurnikov, J.M. Nocek, A.G. Mauk, D.N. Beratan, B.M. Hoffman, J. Am. Chem. Soc. 126 (2004) 2785–2798.
[66] C.C. Moser, J.M. Keske, K. Warncke, R.S. Farid, P.L. Dutton, Nature 355 (1992) 796–802.
[67] A. Bonamore, A. Farina, M. Gattoni, M.E. Schininà, A. Bellelli, A. Boffi, Biochemistry 42 (2003) 5792–5801.
[68] K.L. Dikshit, Y. Orii, N. Navani, S. Patel, H.Y. Huang, B.C. Stark, D.A. Webster, Arch. Biochem. Biophys. 349 (1998) 161–166.
[69] T. Hayashi, A.A. Stuchebrukhov, Proc. Natl. Acad. Sci. U. S. A. 107 (2010) 19157–19162.
[70] A. de la Lande, S. Martí, O. Parisel, V. Moliner, J. Am. Chem. Soc. 129 (2007) 11700–11707.
[71] A. de la Lande, N.S. Babcock, J. Rezác, B.C. Sanders, D.R. Salahub, Proc. Natl. Acad. Sci. U. S. A. 107 (2010) 11799–11804.
[72] A. Jasaitis, M.P. Johansson, M. Wikström, M.H. Vos, M.I. Verkhovsky, Proc. Natl. Acad. Sci. U. S. A. 104 (2007) 20811–20814.
[73] O. Miyashita, M.Y. Okamura, J.N. Onuchic, Proc. Natl. Acad. Sci. U. S. A. 102 (2005) 3558–3563.